J Mater Sci (2007) 42:5318–5326
DOI 10.1007/s10853-006-0960-4

Microhardness of quenched and annealed isotactic polypropylene

Thomas Koch · Sabine Seidler · Erich Halwax · Sigrid Bernstorff

Received: 9 June 2006 / Accepted: 8 September 2006 / Published online: 29 March 2007

Abstract The influence of molecular weight on the microhardness of quenched and subsequently annealed isotactic PP is shown. A clear dependence of microhardness on molecular weight and annealing temperature was detected. Even in the quenched state, where it was difficult to detect morphological differences between the materials, microhardness shows differences. In all states, quenched and annealed, the lower molecular weight samples have the higher hardness values. Up to an annealing temperature of 70 °C the hardness increases only slightly in all samples, above 80 °C a more pronounced increase was observed. For the microhardness of the samples annealed at 140 °C the ratio of the amorphous to the crystalline length is the dominating morphological parameter.

Introduction

Quenching of molten polypropylene to ambient or subambient temperatures leads to a so-called smectic or mesomorphic phase, which can be considered as an intermediate state between the amorphous and the crystalline phase. Several studies [1–6] deal with the description of the nature of this quenched phase. Hypotheses presented include a two-phase system containing amorphous and paracrystalline phases [1], models suggesting that the quenched form contains monoclinic [2] or hexagonal microcrystallites [3] or models based on ordered helical molecules, which are not coherent [4]. Transmission electron microscope (TEM) observations show cluster-like structures having dimensions of about 10 nm [5]. Using atomic force microscope (AFM) regions of different structural order, perhaps consisting of very small particles within a matrix of mesomorphic and/or amorphous structure, were detected [6]. If the quenched form of iPP is annealed it will transform into the monoclinic α-phase [7–9]. This transformation takes place at temperatures higher than 70 °C in relatively short times as determined by wide-angle X-ray diffraction (WAXD) [1, 8]. Annealing for longer times at lower temperatures (40 °C) could also result in the development of the α-phase [9]. This morphological transformation has an influence on the mechanical properties, depending on the annealing temperature. In [10] the tensile behaviour of annealed iPP is discussed whereas in [11] the influence of annealing on the tensile properties and the fracture behaviour, characterized by essential work of fracture method, is shown. The authors found an increase of the elastic modulus [10, 11] as expected, a decrease of essential work and an increase in the plastic work with increasing annealing time [11].

The present work deals with the influence of molecular weight and annealing on the microhardness of quenched isotactic polypropylene. Microhardness testing was chosen for two reasons. Small, thin specimens, which can be produced in a well reproducible quality, can be

T. Koch (✉) · S. Seidler
Institute of Materials Science and Technology, Vienna University of Technology, Favoritenstraße 9-11, Vienna 1040, Austria
e-mail: tkoch@mail.zserv.tuwien.ac.at

S. Seidler
e-mail: sseidler@mail.zserv.tuwien.ac.at

E. Halwax
Institute of Chemical Technologies and Analytics, Vienna University of Technology, Getreidemarkt 9, Vienna 1060, Austria

S. Bernstorff
Sincrotrone Trieste, Strata Statale 14, km 163.5, Basovizza 34012, Italy

characterized by this method. Also, for more than two decades it has been shown that microhardness is a very sensitive method to describe the correlation between structure or morphology and the resulting properties of polymers [12, 13]. Microhardness measurements of polypropylene materials are described extensively in the literature. A linear correlation between microhardness and the degree of crystallinity of PP was shown in [14]. Hardness and modulus of transcrystalline PP detected by Knoop microindentation are described in [15], showing that the values are up to 30% higher when the longer diagonal is oriented perpendicular to the transcrystalline growth direction compared to the parallel orientation of this diagonal. Orientations due to processing conditions were confirmed by microhardness measurements [16, 17]. Microhardness was used for detecting the glass transition temperature of PP [18]. Differences between the α- and the β-phase of polypropylene are shown by indentation testing [19, 20]. Results on the influence of molecular weight and rubber content in PP/EPR blends are given in [21], indicating a small decrease of microhardness with increasing molecular weight. Some papers in the literature describe the correlation between hardness and mechanical properties. Elastic modulus is related to the microhardness by means of a power law [22]. In [23] it is demonstrated that the creep modulus at a defined load and the microhardness have the same time dependence after different ageing times.

Especially for the characterization of thin films or small amounts of material the instrumented indentation test is very suitable, because it does not rely on optical measurement of the impression remaining at the surface and, thus, allows the determination of surface mechanical properties influencing a much smaller volume. This is important for the characterization of thin films due to the necessity to keep the ratio of indentation depth to film thickness smaller than 0.1. Another advantage is that subjective errors, which can result from the optical microscopic measurement of the remaining impressions are eliminated; such errors can play an important role in the case of indentation diameters smaller than 10 μm or when the differences of the diameters between several similar specimens are smaller than 1 μm.

Experimental

Materials

The materials investigated in this study were five isotactic polypropylenes with different molecular weight M_w and a comparable M_w/M_n ratio (see Table 1). Film specimens ($4 \times 3 \times 0.05$ mm^3) were prepared using a hot stage. After heating the sample between thin microscopic slides to 200 °C and keeping the temperature constant for 7 min the film specimens were rapidly transferred into water at room temperature.

Table 1 List of the investigated iPP materials

	M_w (kg/mol)	M_w /M_n	$MFI_{230/2.16}$ (g/10 min)
PP1	885	4.7	0.4
PP2	482	4.9	3.2
PP3	330	4.4	8.6
PP4	230	4.7	27.5
PP5	209	5.0	47.0

Microhardness

Instrumented microhardness tests were done using a Nanoindenter XP, MTS Systems Inc. The indentation depth was 1 μm, the indentation rate 0.05 μm/s. After a holding time of 30 s at maximum load the specimens were unloaded. The indentation hardness H_{IT} was calculated at the maximum load F_{max} with the aid of the contact depth h_c, according to [24]:

$$H_{IT} = \frac{F_{max}}{24.5 h_c^2} \quad (1)$$

with

$$h_c = h_{max} - \varepsilon(h_{max} - h_r) \quad (2)$$

where h_{max} is the indentation depth at F_{max}, h_r is the intercept of the tangent to the unloading curve at maximum load with the depth axis and ε is a constant depending on the indenter shape.

The specimens were glued on metallic sample holders.

Thermal analysis

Differential scanning calorimetry (DSC) measurements were done using a TA Instruments DSC 2920. Sample mass and thickness were 1 mg and 100 μm, respectively. The heating rate was 20 K/min.

For dynamic mechanical thermal analysis (DMTA), carried out with a TA Instruments DMA 2980 in the tensile mode, specimens of the dimensions $15 \times 2 \times 0.15$ mm^3 were used.

X-ray analysis

Small-angle X-ray scattering (SAXS) measurements were carried out at the small angle beamline at the synchrotron radiation source Sincrotrone Trieste, Italy. A Gabriel type

linear detector was mounted at a distance of 2.24 m from the sample. To get a better signal to background ratio 3 samples of 50 μm thickness were stacked. A wavelength of 0.154 nm was used, the beam width was about 700×100 μm^2 and the data collecting time was 5 min. Wide-angle X-ray diffraction (WAXD) was done with a Philips X'Pert Pro instrument using CuK$_\alpha$ radiation in reflexion mode.

FTIR measurements

Fourier transformed infrared spectroscopic (FTIR) investigations were performed on a Bruker Hyperion FTIR microscope in transmission mode. Spectra were recorded at a resolution of 2 cm^{-1}. The state of molecular order can be determined by comparing a ''crystalline'' and a ''reference'' band. Note, that the FTIR method does not distinguish between different ordered phases, such as the crystalline and the mesomorphic phase [25]. The ''crystalline'' bands are sensitive to both ordered phases. Here the absorption peak at 998 cm^{-1} was ascribed to the crystalline or more generally the ordered band. The peak at 973 cm^{-1} was used as reference band; it contains contributions of both the ordered and the amorphous phases and should be almost unaffected. The fraction of ordered (crystalline and/or mesomorphic) phase can be estimated in the following way:

$$X_{\mathrm{FTIR}} = \frac{\varepsilon_{974}}{\varepsilon_{998}} \cdot \frac{A_{998}}{A_{974}} \tag{3}$$

where A_{998} and A_{974} are the absorbencies and ε_{998} and ε_{974} are the extinction coefficients of the ordered and reference bands, respectively. With the help of WAXD crystallinity measurements on annealed samples the extinction ratio was estimated to be 0.68.

Results

Quenched materials

In Fig. 1a the WAXD profiles of the quenched iPP materials are plotted, showing the typical broad peaks at about $2\Theta = 15°$ and 21.5°. The profiles are comparable for the investigated materials. Note, however, that the first peak of 885 kg/mol material (PP1) is somewhat smoother, which could be an indication of a slightly lower ordering state in this material. The diffraction curves were fitted with a convolution of one large asymmetric peak with a maximum at $2\Theta = 16.3°$, taken from the diffractogram of atactic PP and representing the amorphous halo, and two Pearson VII type peaks, representing the mesomorphous phase. In this

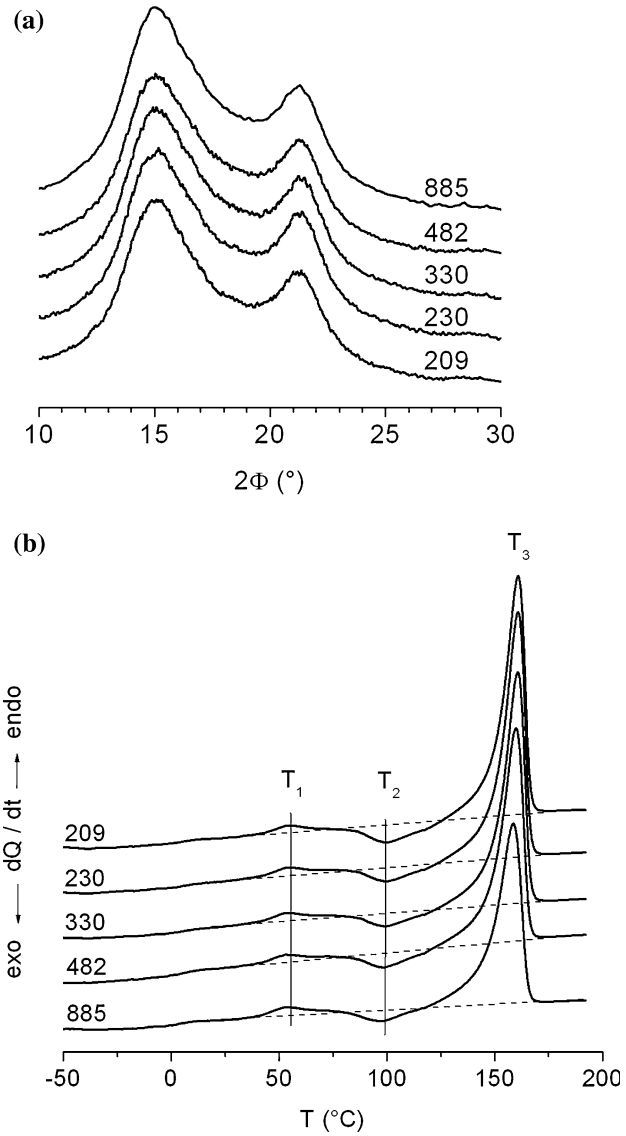

Fig. 1 WAXD profiles (**a**) and DSC thermograms (**b**) of the quenched iPP. The numbers on the curves represent the molecular weight in kg/mol

way the amount of mesomorphic phase was determined to be between 31% and 36%, but without a trend. Maybe that's a problem of the deconvolution method, which could include some error because of a non-sufficient robustness. The obtained values are in good agreement with the results on quenched iPP in [26, 27], but clearly lower than the values presented in [28, 29]. In [28] the mesomorphic phase content was determined also by WAXD. The reason for the higher value of mesomorphic phase content in [28] as compared to our results could be due to the different peak position ($2\Theta = 17°$) and shape of the amorphous halo used by the authors. Moving the halo maximum to higher values of 2Θ and using of a symmetric shape instead of an asymmetric (in our work the asymmetry shape was proven by measurements of atactic PP) as it was done in [28] leads

to a lower peak high and to an underestimation of the amorphous part in the region of small diffraction angles. This results in a higher calculated value of the mesomorphic phase content. In [29] a completely different approach using a sorption method, was chosen. Discrepancies with respect to our results could, thus, be due to the different methodology.

In Fig. 1b the DSC scans obtained from the quenched samples at a heating rate of 20 K/min are shown, exhibiting the typical behaviour during heating with a first endothermic peak at about 55 °C (T_1), followed by an exothermic effect at about 98 °C (T_2) and a sharp endothermic peak at about 160 °C (T_3). As the first two peaks could not be observed for slowly cooled iPP, they can be ascribed to specific phase transitions in the quenched form. The endothermic peak results from the melting process of very small and/or less perfect crystalline regions. This is supported by results in [7] where the independence of the peak position from the heating rate was shown. In [5] the underlying process of this small melting peak is described as a change of the helical structure of chain segments from one hand to another. The following exothermic effect (T_2) corresponds to the recrystallization process where the monoclinic α-phase of PP is formed. The third peak (T_3) corresponds to the melting of the α-crystals. Note, that the true magnitude of all the observed peaks might be different due to the superposition of the transitions. Increasing molecular weight leads to a slight shift of the positions of the two endothermic peaks and the exothermic peak to somewhat lower temperatures (Fig. 1b, Table 2). A higher temperature T_1 results from a higher degree of molecular order in the quenched state. An increase of the (exothermic) temperature T_2 may result from two effects: from a higher degree of physical cross-linking which hinders movement of the molecular chains or/and from a stronger recrystallization, which dominates the superpositioned peak in this region and leads to a shift of this peak to higher temperatures.

Generally it must be pointed out that the materials investigated in this work (quenched in water at room temperature) are equivalent to materials that were annealed at room temperature (see Fig. 2), a fact already described

Table 2 Characteristic temperatures T_1, T_2 and T_3 representing the temperature locations of the first endothermic peak, the exothermic maximum and the second endothermic peak (see Fig. 2)

	T_1 (°C)	T_2 (°C)	T_3 (°C)
PP1	54.0	97.0	158.7
PP2	54.5	98.0	160.0
PP3	54.9	99.0	160.8
PP4	55.2	99.7	161.0
PP5	54.9	99.7	161.0

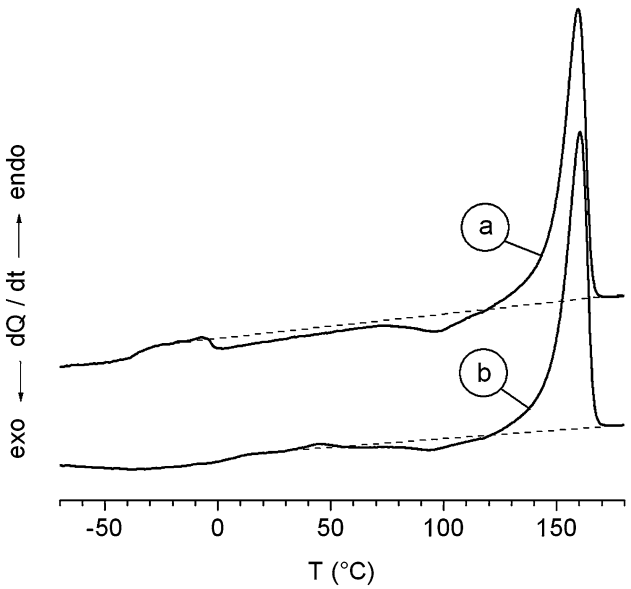

Fig. 2 DSC traces of samples quenched in liquid nitrogen and maintained cool until measurement (**a**) and heated to room temperature before thermal analysis (**b**)

in [30]. The DSC scan of the sample quenched with liquid nitrogen, kept at this temperature and then heated in a cooled DSC starting from –120 °C shows a completely different behaviour in the temperature range below 80 °C compared to that of a sample quenched within liquid nitrogen, held at room temperature for some minutes and then heated. The curve of the latter one is comparable to the heating traces of the samples quenched in water at room temperature.

The SAXS results in terms of the Lorentz-corrected intensity profiles versus the scattering vector (Fig. 3) do not show a visible difference depending on molecular weight; the maximum of the broad peak is located at the same position for all samples (q = 0.7 nm^{-1}) which corresponds to a Bragg spacing of 8.8 nm. The shape of the curves is comparable.

It should be mentioned that density measurements, which are normally very sensitive to morphological changes, did not show a trend for the quenched materials; the values scatter in the range from 885.4 kg/m^3 to 885.7 kg/m^3. From these values and the density of the amorphous form (852 kg/m^3), taken from the middle of the range given in [31], and the density of the mesomorphic phase (916 kg/m^3) [29] a content of mesomorphic phase of about 52% can be calculated. This value is clearly higher than the value derived by WAXD, but is in good agreement with the results presented in [29, 32].

The hardness values of the quenched low molecular weight materials are nearly 20% higher than those of high molecular weight materials (Fig. 4), which proves the high

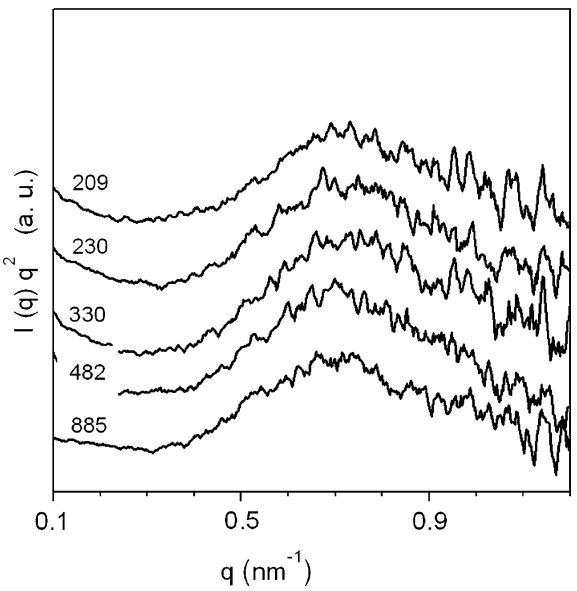

Fig. 3 SAXS profiles of the quenched iPP materials with molecular weights between 209 kg/mol and 885 kg/mol

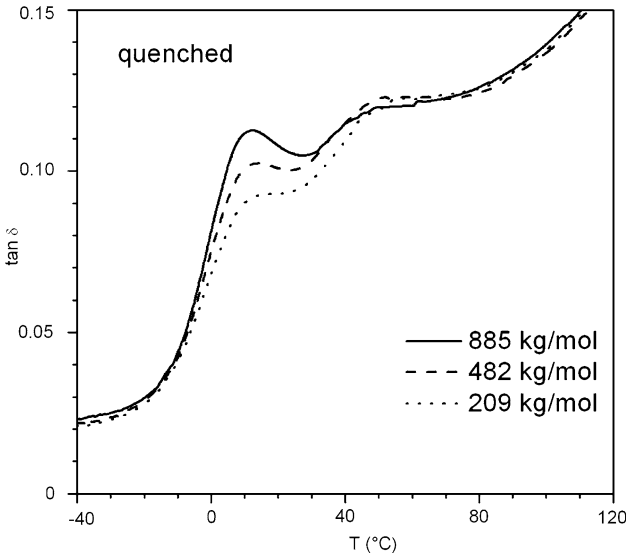

Fig. 5 Mechanical loss tangent tanδ versus temperature for three quenched iPP materials; f = 1 Hz

sensitivity of the microhardness method to structural changes. Higher hardness values for low molecular weight samples were also found in [21], but the quenched specimens in [21] were not smectic, but included strongly crystalline parts. The different mechanical behaviour of the quenched samples is illustrated by the mechanical loss tangent tan δ (Fig. 5). The intensity of the peak at the glass transition temperature decreases with decreasing molecular weight, indicating a stronger hindering of the mobility of the shorter molecular chains maybe due to a stronger physical cross-linking in the short chain materials. This could be also the reason for the higher hardness of these materials.

Although there was no significant difference or trend in the X-ray, DSC and density results for the quenched state, the parameter X_{FTIR}, which represents the degree of molecular order, decreases with molecular weight (Fig. 6). The hardness, therefore, shows a correlation with X_{FTIR}. Note, that the derived values of X_{FTIR} are of the order of the density results. As described in Sect. 2.5 the FTIR measurements do not give information about the kind of ordered phase.

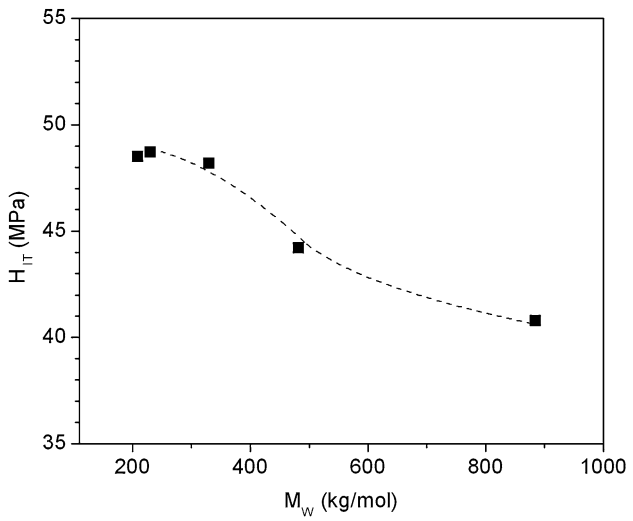

Fig. 4 Indentation hardness of quenched iPP materials in dependence on molecular weight

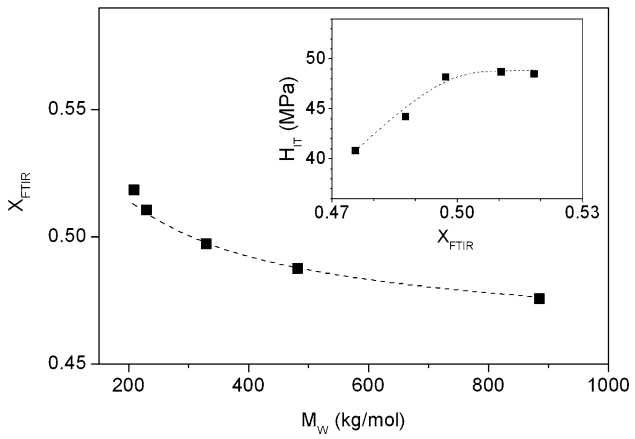

Fig. 6 Degree of molecular order X_{FTIR} of quenched iPP materials in dependence on molecular weight; the insert shows the dependence of indentation hardness on the ordering parameter X_{FTIR}

Annealed materials

If quenched iPP is annealed, large morphological transformations take place, as shown in Fig. 7a–c displaying results from PP3 material with 330 kg/mol. The DSC scans show the typical shift of the first endothermic peak to higher temperatures with increasing annealing temperatures (Fig. 7a), which could be due to the increased perfection of the crystals or of the fold surface, or the development of secondary crystallization with a different perfection. Beginning with the two broad peaks of the quenched sample in the WAXD profiles the development of five strong reflections, representing the reflections of the monoclinic α-phase, can be observed (Fig. 7b). In Fig. 7c the decrease in glass transition temperature (T_g) as derived from the maximum of mechanical loss tangent with increasing annealing temperature is shown. The reason for this behaviour can be given as follows. In the quenched state the microcrystallites hinder the movement of the amorphous phase, they act as physical cross-links [7]. During annealing the smallest and/or less perfect crystallites melt and larger and/or more perfect crystallites can grow. This results in two counterbalanced effects, an increase of crystallinity and a decrease of the physical cross-linking degree of the amorphous phase. In contrast to [7] the magnitude of the relaxation decreases with increasing annealing temperature. Moreover, we did not find a decrease of activation energy as described in [7].

The hardness values H_{IT} show a clear dependence on both the annealing temperature and the molecular weight, as can be seen in the 3-dimensional plot in Fig. 8. As expected an increase of hardness with increasing annealing temperature can be observed. At all annealing temperatures the low molecular weight samples show the higher hardness values. This should be a consequence of the improved ability of the shorter chains to rearrange, that means a better ability to form ordered structures, i.e. crystallites. During annealing the mobility of the shorter chains is higher and therefore ordering and recrystallization are favoured. In the higher molecular weight samples a higher concentration of chain entanglements reduces the possibility of the chains to order. For different polyethylenes crystallized from the melt a similar behaviour was shown in [33]. Up to an annealing temperature of 70 °C the hardness increases only slightly in all samples. Above 80 °C a more pronounced increase can be observed, confirming the morphological changes in the material. The increase of hardness with decreasing molecular weight is approximately linear or slightly progressive for all investigated annealing temperatures. As mentioned above, the lower molecular weight materials show higher absolute hardness values, but also a more pronounced relative increase of hardness over the whole observed temperature range (Fig. 9).

The SAXS peaks become sharper and shift to lower values of the scattering vector q ($=4\pi\sin\Theta/\lambda$, with the scattering angle 2Θ and the wavelength λ) with increasing annealing temperature (Fig. 10). The latter effect indicates an increase in the so-called Bragg or long spacing. Up to an annealing temperature T_a of 80 °C the long spacing L increases moderately with T_a, whereas at T_a = 140 °C a much stronger increase can be observed (Fig. 11). After annealing the high molecular weight samples show larger long spacing values compared to the low molecular weight ones. The dependency of the long spacing on the square root of the molecular weight is nearly linear for the samples annealed at room temperature and 80 °C, a behaviour that has been reported for different quenched semicrystalline polymers in [34]. There are more deviations from linearity for the materials annealed at 140 °C. The slope of the

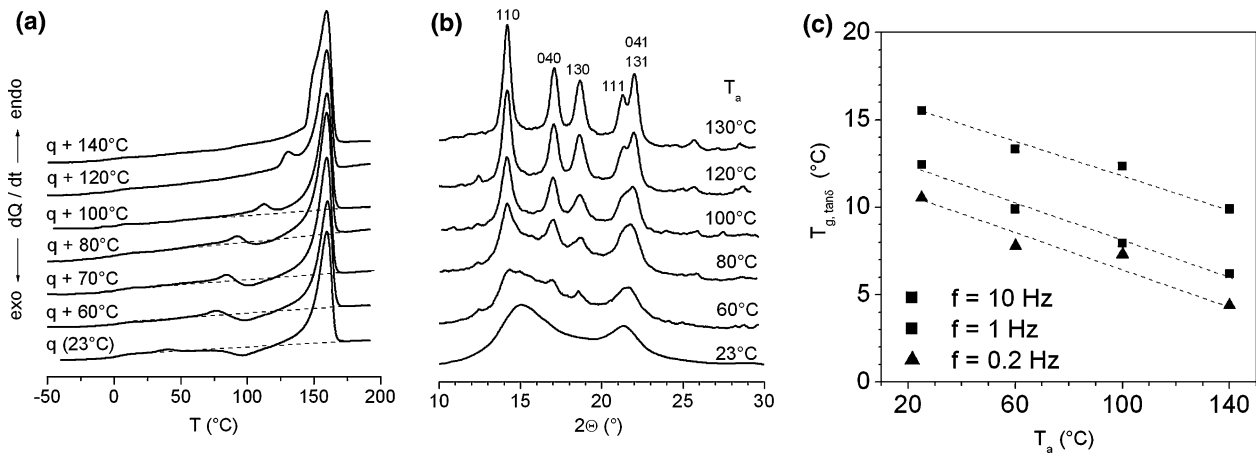

Fig. 7 DSC thermograms (**a**), WAXD profiles (**b**) and glass transition temperatures from tan δ maximums (**c**) of the quenched and annealed PP3 material with 330 kg/mol which was annealed subsequently 1 h at the given temperatures T_a

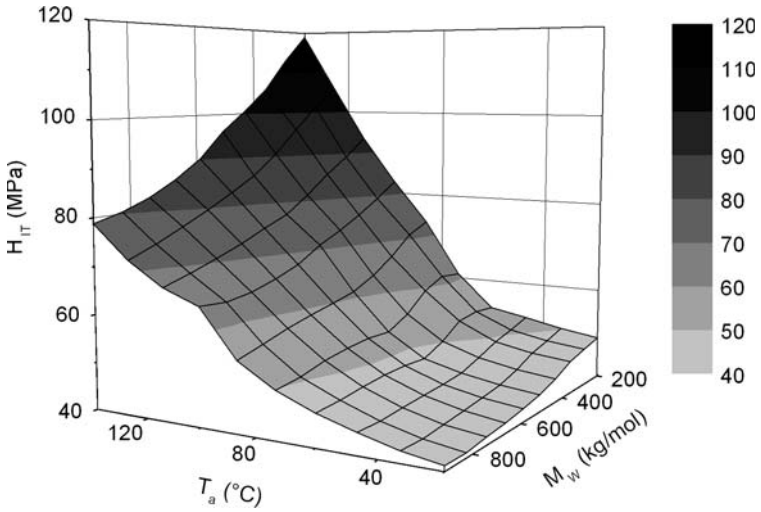

Fig. 8 Indentation hardness of quenched and annealed iPP materials in dependence of annealing temperature and molecular weight

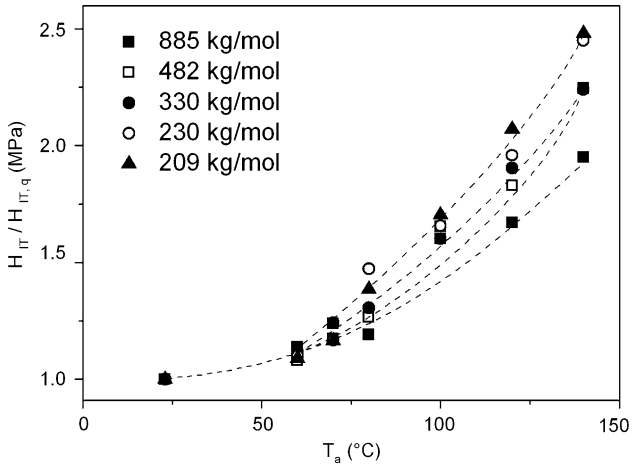

Fig. 9 Relative hardness increase versus annealing temperature

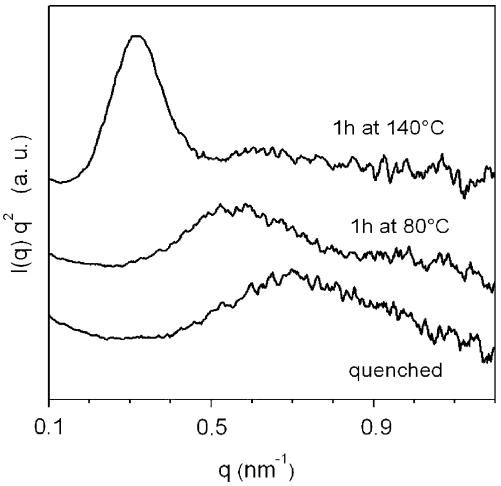

Fig. 10 SAXS profiles of a quenched and annealed iPP

functional connection between L and M_W increases with increasing annealing temperature.

A more detailed analysis of the parameters describing the semi-crystalline structure of the materials annealed at 140 °C, where the mesomorphous phase is absent or can be neglected, is given in Fig. 12. For the investigated materials there is a linear decrease of the crystallinity with the square root of the molecular weight. Besides the long spacing L also the crystalline length l_c ($=X_cL$) and the amorphous length l_a ($=L - l_c$) increase with increasing molecular weight, but the differences in l_a (34%) are much larger than in l_c (14%). Looking at the ratio of amorphous length to crystalline length a strong dependence on molecular weight can be observed. Therefore, it can be concluded that the different hardness values in the annealed samples are mainly caused by the degree of crystallinity and to a larger extent by the amorphous length, especially the ratio of amorphous to crystalline length. The influence of the crystalline length is comparably small. Both, the crystalline and the amorphous length contribute to the increase of long period.

The so-called crystalline hardness of the annealed samples is given by the hardness value of the crystalline phase and can be calculated from the degree of crystallinity. Here, in contrast to [21], it does not remain constant but there is a decrease with molecular weight. This is surprising because the range of molecular weight and the M_w/M_n ratios are comparable. The discrepancies could be due to different initial conditions: mesomorphous phase in our work and about 40% crystallinity in those used in [21]. Following the classical interpretation by Balta-Calleja [12], semicrystalline polymers exhibit a correlation between a thermodynamical parameter b^* and a mechanical parameter b. The parameter b^* can be deduced from the Thomson–Gibbs equation

$$T_m = T_m^0\left(1 - \frac{b*}{l_c}\right) \quad (4)$$

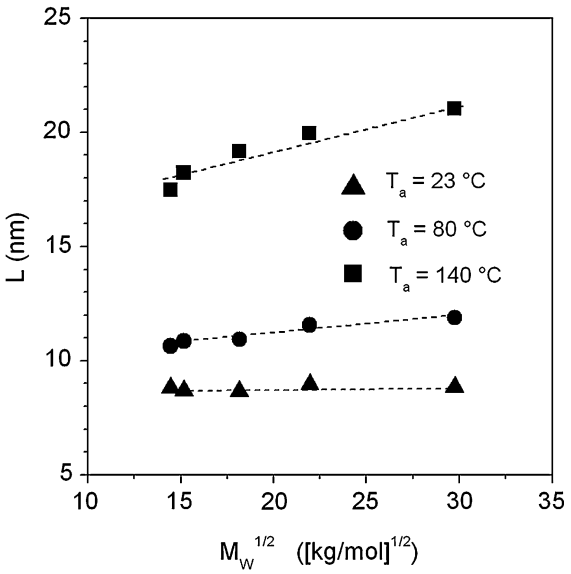

Fig. 11 Long spacing versus the square root of the molecular weight for the quenched and annealed iPP materials. The dashed lines are given for leading the eye

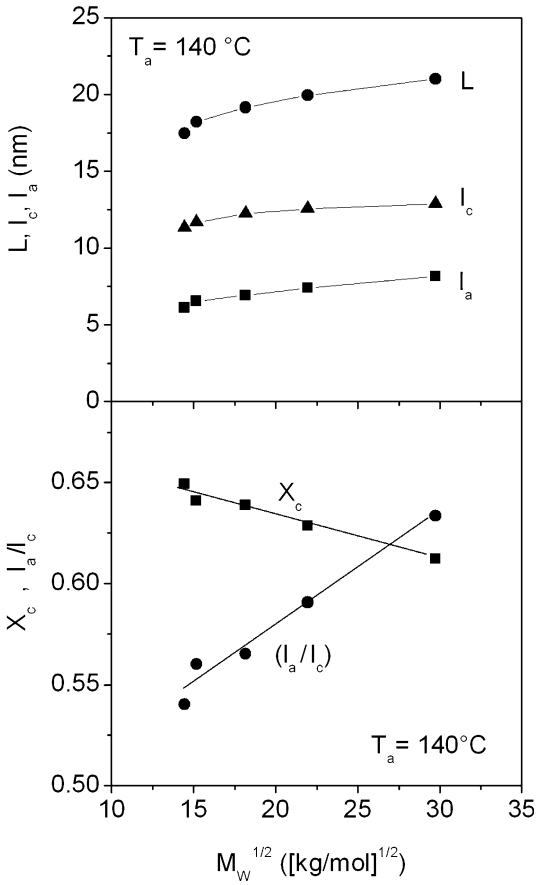

Fig. 12 Long spacing L, crystalline thickness l_c, amorphous thickness l_a, degree of crystallinity X_c and ratio of amorphous to crystalline length (l_a/l_c) versus the square root of the molecular weight for the quenched and annealed iPP materials; annealing temperature T_a = 140 °C

and describes the melting point depression. The α-phase is well developed in samples annealed at 140 °C, the degree of crystallinity is high and the amount of mesomorphous phase should equal zero. Therefore, the DSC curves of these materials are nearly free of recrystallization effects and can be used to determine an adequate melting temperature T_m and to calculate the parameter b^*. The parameter b^* depends on the fold surface free energy σ_e and the theoretical heat of fusion per unit volume of crystal Δh_f^0 ($b^* = 2\sigma_e/\Delta h_f^0$). Using the theoretical equilibrium melting point T_m^0 = 460 K [34] for all the materials, b^* values between 0.67 and 0.81 nm can be calculated. Using Δh_f^0 = 195 J/cm^3 from [35], an increase of the fold surface free energy from 6.6×10^{-2} J/m^2 to 7.9×10^{-2} J/m^2 with increasing molecular weight was found. Since there is a correlation between b^* and the mechanical parameter b, an increase of b^* (and consequently also b) is responsible for a hardness depression. Note, that Eq. 4 is only a simplification, because it neglects effects by lateral surface free energies [6]. In [6] it was reported, that iPP that was quenched and then annealed had a cluster-like morphology in contrast to the typical lamellar morphology of slowly cooled iPP and that the parameters crystallinity, heat of fusion, melting temperature and the structural data obtained by WAXD and SAXS are insensitive to these differences. Nevertheless the trend of the calculated values b^* shown above should not be influenced significantly by these different morphologies.

Conclusions

In the present work an analysis on the influence of molecular weight and annealing on the microhardness of quenched iPP was shown. Even in the mesomorphic state, which is achieved by quenching, there is a distinct dependence of microhardness on molecular weight. The hardness decreases with increasing molecular weight. Whereas WAXD, SAXS and density data show no significant difference nor trend for the materials in the quenched state, the order parameter derived from FTIR analyses increases with decreasing molecular weight.

Annealing of the quenched materials leads to transformations of the morphology resulting in an increase of microhardness. Up to an annealing temperature of 70 °C the hardness increases only slightly, annealing at higher temperatures results in a much greater increase of hardness. In the whole temperature range investigated the lower molecular weight samples show the higher hardness values

due to a improved ability of the short chains to rearrange in crystalline structures. The hardness of the annealed (T_a = 140 °C) samples is controlled by the ratio of amorphous to crystalline length. Also, an increase of the fold surface free energy with increasing molecular weight could be demonstrated.

Acknowledgement Financial support by the European Union for the Elettra synchrotron measurements is gratefully acknowledged.

References

1. Zannetti R, Celotti G, Fichera A, Francesconi R (1969) Makromol Chem 128:137
2. Bodor G, Grell M, Kello A (1964) Faserforsch Textil Technol 15:527
3. Gezowich DM, Geil PH (1968) Polym Eng Sci 8:202
4. Hendra PJ, Vile J, Willis HA, Zichy V, Cudby MEA (1984) Polymer 25:785
5. Wang Z-G, Hsiao BS, Srinivas S, Brown GM, Tsou AH, Cheng SZD, Stein RS (2001) Polymer 42:7561
6. Androsch R, Wunderlich B (2001) Macromolecules 34:5950
7. Alberola N, Fugier M, Petit D, Fillon B (1995) J Mater Sci 30:1187
8. Grubb DT, Yoon DY (1986) Polym Commun 27:84
9. Gerardi F, Piccarolo S, Martorana A, Sapoundjieva D (1997) Macromol Chem Phys 198:3979
10. Alberola N, Fugier M, Petit D, Fillon B (1995) J Mater Sci 30:860
11. Ferrer-Balas D, Maspoch ML, Martinez AB, Santana OO (2001) Polymer 42:1697
12. Baltá-Calleja FJ, Fakirov S (2000) Microhardness of polymers. Cambridge University Press, Cambridge
13. Baltá-Calleja FJ (1985) Adv Polym Sci 66:117
14. Martínez-Salazar J, García Tijero JM, Baltá-Calleja FJ (1988) J Mater Sci 23:862
15. Amitay-Sadovsky E, Wagner HD (1999) J Polym Sci B 37:523
16. Osawa S, Porter RS (1996) Polymer 37:2095
17. Schreyer GW, Zwinzscher K, Lüpke T, Wutzler A (1998) Kaut Gummi Kunstst 51:35
18. Martin B, Perena JM, Pastor JM, de Saja JA (1986) J Mater Sci Lett 5:1027
19. Labour T, Ferry L, Gauthier C, Hajji P, Vigier G (1999) J Appl Polym Sci 74:195
20. Seidler S, Koch T (2004) Macromol Symp 217:329
21. Flores A, Aurrekoetxea J, Gensler R, Kausch HH, Balta-Calleja FJ (1998) Colloid Polym Sci 276:786
22. Lorenzo V, Perena JM, Fatou JG (1989) J Mater Sci Lett 8:1455
23. Chua SM, Henderson PJ (1991) J Mater Sci Lett 10:1379
24. Oliver WC, Pharr GM (1992) J Mater Res 7:1564
25. Lamberti G, Brucato V (2003) J Polym Sci Phys 41:998
26. Martorana A, Piccarolo S, Scichilone F (1997) Macromol Chem Phys 198:597
27. Scharnowski D (2005) PhD thesis, University Halle-Wittenberg
28. McAllister PB, Carter TJ, Hinde RM (1978) J Polym Sci Phys 16:49
29. Vittoria V (1986) J Polym Sci Phys 24:451
30. Caldas V, Brown GR, Nohr RS, MacDonald JG, Raboin LE (1994) Polymer 35:899
31. Phillips RA, Wolkowicz MD (2005) In: Pasquini N (ed) Polypopylene handbook. Hanser, Munich, p 163
32. Vittoria V (1989) J Macromol Sci Phys B 28:97
33. Baltá-Calleja FJ, Santa Cruz C, Bayer RK, Kilian HG (1990) Colloid Polym Sci 268:440
34. Robelin-Souffache E, Rault J (1989) Macromolecules 22:3581
35. Varga J (1995) In: Karger-Kocsis J (ed) Polypropylene. Structure, blends and composites, vol 1. Chapman & Hall